metals

MDPI

Article

Investigation on Vanadium Chemistry in Basic-Oxygen-Furnace (BOF) Slags—A First Approach

Sophie Wunderlich [1,*], Thomas Schirmer [2] and Ursula E. A. Fittschen [1]

[1] Institute of Inorganic and Analytical Chemistry, Clausthal University of Technology, Arnold-Sommerfeld Str. 4, 38678 Clausthal-Zellerfeld, Germany; ursula.fittschen@tu-clausthal.de
[2] Institute of Disposal Research, Mineralogy, Geochemistry, Salt Deposits, Adolph Roemerstr. 2a, 38678 Clausthal-Zellerfeld, Germany; thomas.schirmer@tu-clausthal.de
* Correspondence: sophie.wunderlich@tu-clausthal.de

Abstract: Basic oxygen furnace (BOF) slag accounts for the majority of all residual materials produced during steelmaking and may typically contain certain transition metals. Vanadium, in particular, came into focus in recent years because of its potential environmental toxicity as well as its economic value. This study addresses the vanadium chemistry in BOF slags to better understand its recovery and save handling of the waste stream. The experimental results from the electron probe microanalysis (EPMA) study show that vanadium is preferably incorporated in calcium orthosilicate-like compounds (COS), with two variations occurring, a low vanadium COS (COS-Si) (approx. 1 wt.%), and a high vanadium COS (COS-V) (up to 18 wt.%). Additionally, vanadium is incorporated in dicalcium ferrite-like compounds (DFS) with an average amount of 3 wt.%. Using powder x-ray diffraction analysis (PXRD), EPMA, and virtual component models, stoichiometric formulas of the main vanadium-bearing phases were postulated. The stoichiometries give an estimate of the oxidation states of vanadium in the respective hosts. According to these results, trivalent vanadium is incorporated on the Fe-position in dicalcium ferrite solid solution (DFS), and V^{4+} and V^{5+} are incorporated on the Si-position of the COS.

Keywords: BOF-slag; steel slag; vanadium; calcium orthosilicate; electron probe microanalysis (EPMA)

Citation: Wunderlich, S.; Schirmer, T.; Fittschen, U.E.A. Investigation on Vanadium Chemistry in Basic-Oxygen-Furnace (BOF) Slags—A First Approach. *Metals* **2021**, *11*, 1869. https://doi.org/10.3390/met11111869

Academic Editor: Chengjun Liu

Received: 31 October 2021
Accepted: 18 November 2021
Published: 20 November 2021

1. Introduction

During steel production, various byproducts are generated. Besides dust and sludges, slags are the main side-products. Slags can be divided into blast furnace (BF) slags produced during the reduction of iron ore in the blast furnace and steel slags generated during steel production. Depending on the type of steel mill, steel slags originate either in an electric arc furnace (EAF) or in a basic oxygen furnace (BOF). Taking the EU as an example, in 2019, 93,850,800 t of steel were produced in a BOF compared to 64,949,200 t in an EAF [1]. Typically, around 10% slag is produced per ton of steel [2]. Therefore, BOF slag accounts in terms of quantity for the largest share of the byproducts of the steel industry. In an integrated steel mill, where steel is produced via the BF-BOF-route, iron ore is reduced with coal in a blast furnace. The resulting high-carbon-containing pig iron is oxidized together with cooling scrap and slag formers such as lime in the BOF, removing excess carbon and achieving the ideal carbon content of the desired steel product. During this process, BOF slag is formed on top of the steel bath. The main purpose of BOF slag is, on the one hand protecting the steel bath from oxidation and, on the other hand, removing unwanted accompanying elements from the metal melt. Iron ore can be accompanied by sulfur, silicon, aluminum, magnesium, and calcium but also transition metals such as manganese, vanadium, and chromium. Vanadium, in particular, is usually entirely transferred into the slag, resulting in a vanadium content of some BOF-slags of approx. 2.8 wt.% (resp. 5 wt.% V_2O_5) [3].

In recent years, especially vanadium gained more and more attention due to the environmental toxicity of certain compounds and oxidation states, as well as increasing global demand. Usually, vanadium is used as an alloying element in steel production, leading to the high-strength steel used in the aerospace industry or as a catalyst in the chemical industry. Additionally, it is utilized in vanadium redox flow batteries for energy storage [4,5].

Since some BOF-slags show a relatively high vanadium content compared to typical natural vanadium sources like titanomagnetite ores, vanadium-bearing sandstones, or black shales with vanadium concentrations of 0.2–1.7 wt.% V_2O_5 [4] those slags can be a viable source of vanadium for the applications mentioned above. To recover vanadium from BOF slags, a basic understanding of vanadium chemistry in these industrial melts is elementary. It enables developing strategies, e.g., communition, flotation, or extraction.

The formation of vanadium compounds in slags and the main properties of these compounds depend strongly on the particular oxidation state of the element. Vanadium is a first subgroup transition metal and can be present in many oxidation states, where the most common are +2–+5 [6]. In solid compounds, it can adopt different coordination numbers and geometries. This variety of oxidation states complicates the understanding of compound formation in complex melts.

The formation of vanadium-bearing compounds in industrial melts, such as BOF slag, is to some extend comparable to these processes in natural analogs like magmas, preferably basaltic melts. In an aerobic environment, V^{2+} is unstable, while V^{3+} shows higher stability but tends to gradual oxidation exposed to air or dissolved oxygen. In waters exposed to atmospheric oxygen, V^{5+} is the predominant form, whereas in reducing environments, V^{4+} occurs [5]. Many authors, e.g., [7–9], describe the occurrence of vanadium oxidation states in basaltic melts. Toplis and Corge [7], for example, postulated a coexistence of V^{3+}, $V^{4+,}$ and V^{5+} under certain oxygen fugacity conditions in the melt, while V^{3+} and V^{4+} are preferably incorporated in crystal structures (e.g., clinopyroxenes). In comparison to that of basaltic melts, after the BOF process, vanadium is assumed to be predominately present in V^{3+} and/or V^{4+} and/or V^{5+}, leading to a similar distribution [10].

Slag phases are often described as solid solutions with a relatively broad scattering in the chemical composition due to the fast cooling rate. They are usually not attaining a thermodynamic equilibrium during solidification. Additionally, the prevailing oxygen partial pressure and the chemical composition define the mineralogy [11]. Many authors mentioned that vanadium in BOF slags is preferentially incorporated in calcium orthosilicates, dicalcium ferrites, and spinels. Especially calcium orthosilicates like larnite (Ca_2SiO_4) play an important role because of the potential incorporation of phosphorous and vanadium [12–15].

As mentioned above, BOF-slags account for most byproducts generated during steel production and may contain vanadium in specific proportions. Vanadium is becoming more and more important for legislators but also for research and industry. Therefore, the understanding of vanadium chemistry in BOF slags is crucial to further enable, on the one hand, sustainable marketing of steel slags and, on the other hand, to secure the raw material situation through vanadium recovery.

Accordingly, this study identifies vanadium compounds in a typical BOF-slag, describing vanadium distributions over several phases. The results of the investigations are intended to improve the understanding of the formation of vanadium-bearing compounds and predict the general behavior of vanadium in industrially produced melts. Our calculations using a virtual phase concept provide a first hypothesis of the general vanadium incorporating phase formulas giving an estimate of the oxidation states. The method of modeling with virtual components, based on PXRD and EPMA data, was applied to BOF slags for the first time in this study. Moreover, this hypothesis about vanadium chemistry in BOF-slags forms the basis for future experiments.

2. Materials and Methods

2.1. Materials

Since this study requires accurate identification of vanadium and vanadium-bearing (mineral) compounds, a slag sample with high vanadium concentration (typically BOF slags contain between 0.1–2.8 wt.% V) of 1.9 wt.% V was selected. This concentration is well above the limit of detection of the EPMA of about 130 µg/g. Vanadium in steel slags typically enters the system either through scrap charge or through the ores used. Apatite-bearing magnetite ores, in particular, can carry a considerable amount of vanadium along with phosphorus, fluorine, or chlorine [16]. In slags, pure components are rarely present; rather common are solid solutions or phases containing a relatively high amount of impurities. In addition, the contents of transition metals, such as vanadium or chromium, are usually so low that they do not form phases of their own. The slag investigated in this study originates from an actual metallurgical process; it is not a synthetic slag with precisely defined formation parameters.

2.2. Methods

2.2.1. Bulk Chemical Analysis

The elemental composition of the sample was determined with inductively coupled plasma optical emission spectroscopy (ICP OES), (Plasma Quant 9000 Elite, Analytik Jena GmbH, Konrad-Zuse-Str. 1, 07745 Jena, Germany). To prepare the measurement solutions, 0.1 g of sample was melted with lithium tetraborate (Merck KGaA, Darmstadt, Germany) (0.5 g) in a graphite crucible at 950 °C. After 15 min, the crucible is removed, swirled until the melt forms a bead, and emptied while still hot into a plastic cup filled with 40 mL HNO_3 (3%, Merck KGaA, Darmstadt, Germany). Until the melt is completely dissolved, the sample is placed on a magnetic stirrer. The sample is filtered into a 1,000 mL volumetric flask which is filled up to the mark with deionized water. This sample solution was analyzed in duplicates with ICP-OES.

2.2.2. X-ray Powder Diffraction (PXRD)

The bulk mineralogical composition was analyzed by PXRD in Bragg Brentano geometry using a PANalytical Aeris (Malvern PANalytical GmbH, Nürnberger Str. 113, 34123 Kassel, Germany) diffractometer and Co$K\alpha_1$ radiation. The samples were ground in a vibrating disk mill and sieved at 50 µm. Grinding was repeated until no particles larger than 50 µm were present. The samples (approx. 2.5 g) were manually pressed into a backloading sample holder. For qualitative phase analysis, the program package High Score Plus (Malvern PANalytical GmbH, Nürnberger Str. 113, 34123 Kassel, Germany) was used, Rietveld refinement was performed with the program package Fullprof [17].

2.2.3. Electron Probe Microanalysis (EPMA)

The elemental distribution throughout the sample and its internal structure was analyzed by EPMA, using a Cameca SX^{FIVE} FE (Field Emission) electron probe, with five wavelength dispersive spectrometers (CAMECA SAS, 29, quai des Grésillons, 92230 Gennevielliers, Cedex, France). The samples were polished and embedded in epoxy resin and coated with carbon. BSE (Z) and EDX analysis were used for the initial orientation and classification of the sample. For a quantitative analysis of the selected points, WDX was applied. The Kα-lines of the elements Na, Mg, Al, Si, P, K, Ca, Ti, Cr, Mn, Fe, Co, and Ni were used for the determination. The wavelength dispersive X-ray fluorescence spectrometers were calibrated with an appropriate set of standards and analyzing crystals, with reference materials from P&H Development Ltd. (Glossop, Derbyshire, UK) and Astimex Standards Ltd. (Toronto, ON, Canada). Measurement parameters were set to 15 kV and 30 nA, with a beam diameter substantially below 1 µm. To evaluate the measured intensities, the X-PHI-Model was used [18].

2.2.4. Modeling

To estimate possible lattice sites and oxidations states of vanadium in its hosting compounds, molecular formulas of the vanadium-containing phases were calculated as follows:

Using a qualitative phase analysis of the bulk with PXRD, the main slag components are identified based on their crystal lattice using an appropriate XRD pattern database. Then, applying EPMA analysis, the impurities in the main phases of the microstructure are determined. Thus, the basis for the modeling performed in this study is, on the one hand, the crystal system of the main phases (hosts), determined via PXRD, and, on the other hand, the knowledge about the incorporated impurity atoms, determined via EPMA.

For each relevant element/impurity, a virtual component (VC) is selected. A prerequisite for these virtual components is a crystal system analogous to the main carrier phase, thus enabling a virtual solid solution. Taking Ca_2SiO_4 as an example, virtual components could be X_2SiO_4-compounds, Ca_2YO_4-compounds, or multiples thereof, with X and Y being the impurities measured via EPMA.

The fraction (F) of the VCs (e.g., X_2SiO_4) in a grain with an assigned main phase (e.g., Ca_2SiO_4) and concentration of an impurity (determined by EPMA) is calculated according to the following equation:

$$F(\mathrm{VC}) = \frac{c_{Igrain}}{c_{Ivirtc.}}$$

where c_{Igrain} is the impurity (e.g., vanadium) content in the grain measured with EPMA in wt.% and $c_{Ivirtc.}$ is the proportion of the impurity in the VC in wt.%.

The multiplication of the factors of all VCs with the respective stoichiometric indices results in an overall stoichiometric formula for each slag component. These calculations deliver results for the parameters that cannot be obtained by EPMA (in this case, the oxidation state of vanadium).

3. Results

3.1. Bulk Chemical Analysis

The bulk elemental composition of the slag is a piece of crucial information evaluating the relevance of the phases identified in the microstructure and with PXRD. The concentration of vanadium in the bulk material allows an estimation of the concentration of vanadium-bearing phases in the entire slag. The amount of amorphous material may also be assessed by comparing bulk elemental composition with the PXRD results. The bulk chemical composition of a BOF-slag was determined by digestion-assisted ICP-OES analysis. The results of the bulk chemical analysis are shown in Table 1. Insoluble residues on the filter could not be observed. Major elements (besides oxygen) are Ca and Fe; minor elements are Si, Mg, and Al, both as expected for this kind of slag. The vanadium concentration is relatively high with 1.9 wt.%. The presence of Cr, P, Mn, and Ti is common in BOF-slags.

Table 1. Bulk chemical analysis of selected BOF-slag (wt.%), N = 4. Standard deviations in brackets.

Ca	Fe	Si	Mg	Al	Cr	P	Mn	V	Ti
29.7 (0.3)	15.8 (0.3)	5.26 (0.15)	5.18 (0.16)	0.60 (0.06)	0.48 (0.05)	0.221 (0.012)	2.23 (0.02)	1.90 (0.04)	0.76 (0.02)

3.2. X-ray Powder Diffraction

The phase composition plays a decisive role because it ultimately determines the properties of the slag (e.g., volume stability, leaching behavior, etc.). Typically, the phases in slags form solid solutions. Therefore, their composition is highly variable and can only be described by a mixture of endmembers or constitutive phases, defined by their crystal symmetry. Here, PXRD was applied to determine the main phases. For quantitative phase

analysis, Rietveld refinement was used. The COD (crystallographic open database) was applied for references [19].

The main (or base) compounds determined with PXRD in average are Ca_2SiO_4 (larnite or calcium orthosilicate, resp.), accounting for approx. 40 wt.%, $Ca_2Fe_2O_5$ (srebrodolskite or dicalcium ferrite, resp.), approx. 20 wt.% and $Ca(OH)_2$ (portlandite), approx. 11 wt.%. Accessory phases are spinel solid solution (up to 5 wt.%), $CaCO_3$ (calcite, approx. 4 wt.%), and the primitive oxides CaO (free lime, approx. 5 wt.%), FeO (wuestite), and MgO (periclase), together approx. 15 wt.%. The pattern shows a significant peak broadening in the regions of $30° \leq 2\theta \leq 40°$, indicating a certain amount of amorphous phases as well as the incorporation of impurities. Taking the error of the Rietveld refinement into account, which can be estimated to be 5–10% due to the high number of phases, the quantitative analysis is in the range of the elemental analysis with ICP OES (Table 1).

The concentrations of the base phases determined by PXRD and Rietveld modeling are summarized in Table 2.

Table 2. Main phases determined with PXRD. Quantitative results (wt.%) acquired via Rietveld refinement.

Ca_2SiO_4	$Ca_2Fe_2O_5$	(Fe,Mg)O	CaO	$Ca(OH)_2$	$CaCO_3$	Spinel
45	14	19	3	12	6	1

3.3. EPMA—Analysis and Calculations

Based on PXRD, the major slag components calcium orthosilicate (β-Ca_2SiO_4, hereinafter referred to as calcium-orthosilicate-like compound (COS)), dicalcium ferrite ($Ca_2Fe_2O_5$, hereinafter referred to as dicalcium ferrite solid solution (DFS)), wuestite-like primitive oxides (Fe(Ca,Mg))O (WLO)) and portlandite were identified. Accessory phases are calcite, lime, and spinel.

EPMA was used to obtain a general overview of the samples' microstructure in terms of its morphology, grain size distribution, homogeneity, and the proportion of crystalline or amorphous content. Subsequently, the elemental distributions over individual grains were characterized. In the BSE(Z)-micrograph, shown in Figure 1, four different major phases can be distinguished:

−A: Calcium-orthosilicate-like compound (COS, X_2YO_4) with Ca, Si, and less V and P).
−B/C: Wüstite-like primitive oxides (WLO, XO with Ca, Mg, and Fe).
−D: Dicalcium ferrite solid solution (DFS, $X_2Y_2O_5$ with Ca, Fe, and less Al, Mg, V, Cr, and Mn).

The grains of component A are up to 50 µm in diameter and exhibit a hypidiomorphic habitus, partly with a distinct cleavage. Additionally, they show alteration at the outer rim. The grain morphology of component B is similar to A but with significantly more alteration distributed over the entire grain. Component C shows a xenomorphic grain morphology and fills the gaps between components A and B. Component D appears as a lath-shaped grain that apparently, together with C, spans the matrix. Alteration of the phases originates most probably through the water-based preparation of the polished sections.

The elemental results from several point measurements over the entire sample were grouped according to the assigned grain type. The arithmetic mean values of the elemental concentrations were calculated for each grain type (Table 3).

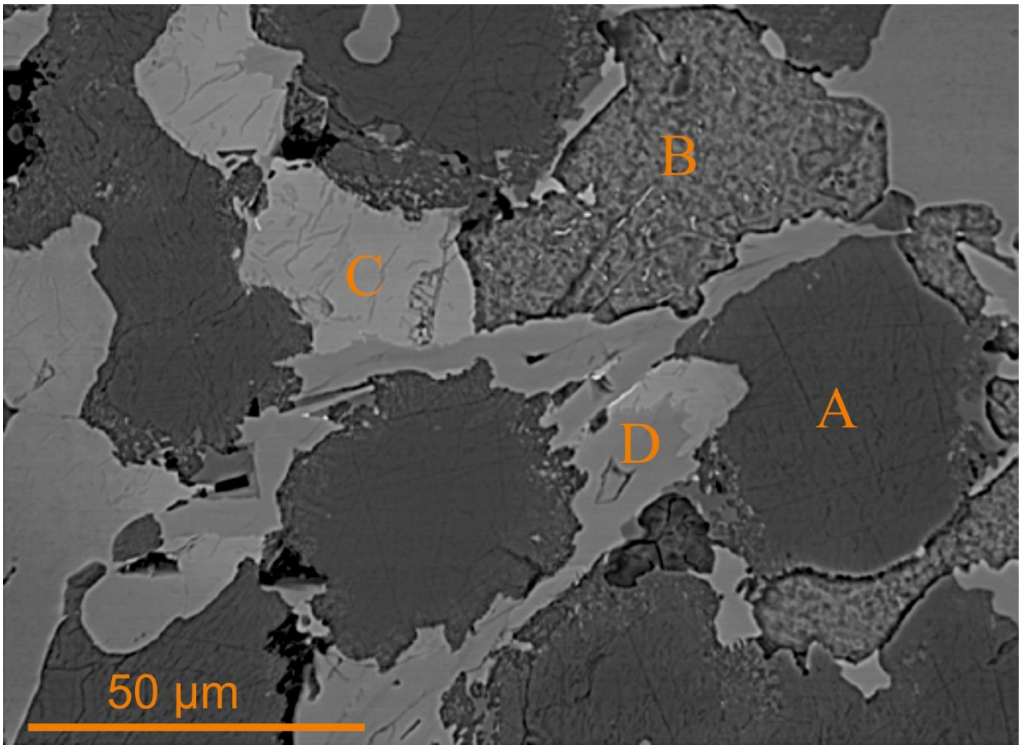

Figure 1. BSE (Z) micrograph of analyzed BOF slag.

Table 3. Elemental composition of main slag phases COS (A); N = 40, CaO (B); N = 28, solid solution between MgO and FeO, (Mg,Fe)O (C); N = 33 and DFS (D); N = 26. Obtained via EPMA WDX. Values and standard deviation, in brackets, given in wt.%.

	A-Type	B-Type	C-Type	D-Type
Ca	42 (4)	54.4 (1.4)	1.6 (0.6)	30.7 (0.5)
Fe	0.8 (0.4)	11.1 (0.5)	47 (5)	26 (3)
Si	9 (4)	0.09 (0.03)	0.022 (0.009)	0.46 (0.11)
V	8 (8)	0.033 (0.009)	0.09 (0.02)	2.9 (0.2)
Cr	0.3 (0.2)	0.10 (0.05)	1.3 (0.6)	1.4 (0.9)
P	0.7 (0.1)	0.020 (0.005)	-	-
O	33 (3)	27.1 (0.2)	28.5 (1.5)	27.0 (0.5)
Al	0.10 (0.05)	0.006 (0.003)	0.013 (0.007)	2.4 (0.2)
Mg	-	1.0 (0.3)	18 (4)	0.43 (0.11)
Mn	0.05 (0.02)	4.7 (0.3)	6.5 (0.9)	0.54 (0.07)
Ti	0.24 (0.09)	-	-	3.3 (1.0)

Via WD-EPMA point measurements, the different phases were assessed and compared with the PXRD measurement. Grain-A in Figure 1 was identified being COS, grain-B being CaO, C-grains being solid solution between MgO and FeO, (Mg,Fe)O, and D-grains being DFS. B-type grains also show a spotty appearance, which can also be attributed to advanced

hydration (formation of $Ca(OH)_2$). The next step is to postulate the stoichiometric composition of these vanadium-bearing compounds by virtual component modeling according to the formula described in Section 2.2.4.

3.3.1. Modeling of the Composition of the Different Grain Types—Characterization of COS

The type A grains (Figure 1) are best characterized by a calcium-orthosilicate-like structure. Looking more closely at the individual A-type grains, sub-types can be distinguished, either rich in Si (COS-Si A-type) or rich in V (COS-V A-type). The average elemental concentration of these grains is given in Table 4.

Table 4. Average concentrations of main elements (in wt.%) in different COS-grains (A.1–A.4), measured with EPMA, WDX (standard deviation in brackets (N = 7)). As a comparison, composition of pure calcium orthosilicate is listed as well.

	COS-Si		**COS-V**		
Grain	**A.1**	**A.2**	**A.3**	**A.4**	**Pure Ca_2SiO_4**
Ca	45.3 (0.4)	45.5 (0.3)	41.7 (0.6)	41.9 (0.3)	46.54
Fe	0.96 (0.07)	1.0 (0.3)	0.6 (0.2)	0.8 (0.5)	-
Si	13.5 (0.4)	13.7 (0.3)	4.89 (0.13)	4.8 (0.2)	16.31
V	1.3 (0.4)	1.1 (0.2)	16.6 (0.4)	16.2 (0.3)	-
Cr	0.082 (0.011)	0.092 (0.013)	0.526 (0.010)	0.50 (0.03)	-
P	0.58 (0.02)	0.59 (0.02)	0.70 (0.07)	0.72 (0.11)	-
O	35.4 (0.3)	35.7 (0.3)	32.8 (0.3)	32.8 (0.3)	30.08

Based on the Ca/Si ratio of the COS-Si type, Ca_2SiO_4 can be assumed to be the main structure. Pure calcium orthosilicate, with the structural formula Ca_2SiO_4, contains 46.539 wt.% Ca, 16.306 wt.% Si, and 37.155 wt.% O. If this ideal distribution is compared to the measured mass balance in one of the grains (exemplarily shown for two COS-Si type grains A.1 and A.2 and two COS-V type grains A.3 and A.4), considerable differences are evident (Table 4).

Apart from lower silicon content and minor concentrations of phosphorous, vanadium, and iron, A.1 and A.2 are very similar to pure Ca_2SiO_4 (COS-Si, Table 4). In contrast, the measurements A.3 and A.4 (Table 4) show significant deviations for Si as well as for Ca content compared to the ideal ones in Ca_2SiO_4 with strong enrichment of vanadium (COS-V, in some measurements up to 18 wt.%) in combination with depletion of silicon.

The COS in the sample is understood to be a solid solution, which can be described by a mixture of several virtual components. The rhombohedral crystal system of COS is the main criterion for selecting the virtual components. The miscibility of Ca_2SiO_4 with, e.g., $Ca_3(PO_4)_2$ is well known [20]. Assuming P^{5+} occupies the Si^{4+} position, a substitution according to the principle of coupled substitution [21] would be consequential, i.e., $Si^{4+} + Si^{4+} \rightarrow V^{3+} + P^{5+}$. However, compounds structurally similar to calcium orthosilicates and incorporating V^{3+} are rarely known. Additionally, the ratio of vanadium to phosphorous in COS is clearly on the vanadium side, making a diadochic replacement according to the equation mentioned above unplausible. Instead, a combination of the virtual components Ca_2SiO_4, Ca_2VO_4, $Ca_3(VO_4)_2$, $Ca_3(PO_4)_2$, Ca_2CrO_4, and Fe_2SiO_4 yielded a stoichiometric formula describing the experimentally derived concentration. The fraction of each component is determined as described in Section 2.2.4. The fractions are summed up to give a universal formula which is subsequently normalized to four oxygen atoms. The base compound calcium orthosilicate defines the number of oxygen atoms.

Finally, the procedure described above leads to the following stoichiometric formulas:

Low vanadium content (COS-Si): $(Ca_{1.91}, Fe^{2+}{}_{0.04})_{1.95}$ $(V^{4+}{}_{0.02}, V^{5+}{}_{0.04}, P^{5+}{}_{0.06}, Si_{0.88})_{1.0}$ O_4

High vanadium content (COS-V): $(Ca_{1.90}, Fe^{2+}{}_{0.03})_{1.93}$ $(V^{4+}{}_{0.55}, V^{5+}{}_{0.07}, P^{5+}{}_{0.07}, Cr^{4+}{}_{0.02}, Si_{0.28})_{1.0}$ O_4

The calculations using these virtual compounds still lead to a stoichiometric excess of calcium of about 5% in the COS-Si and about 2% in the COS-V.

As an example, results from this model calculation for the grains A.2 and A.4 are shown in Table 5. The excess of Ca is addressed with the virtual compound CaO. The complete calculations for the other grains (A.1, A.3) are listed in Appendix A.

Table 5. Calculated fractions of virtual components postulated from elemental composition determined by EPMA analysis of grains of the A.2-type (COS-Si) and A.4 (COS-V). Chemical formulas of virtual components are given in header row. Corresponding fraction is abbreviated with F. Additionally, elemental concentration in grain arising from individual component fraction is given. Optimized composition is shown in last column. Excess calcium content is expressed as CaO.

	Meas. A.2	**Ca_2SiO_4**	**Ca_2VO_4**	**$Ca_3(VO_4)_2$**	**$Ca_3(PO_4)_2$**	**Fe_2SiO_4**		**Opt.**	**CaO**
F		0.824853	0.023171	0.017010	0.029576	0.018244			0.061952
Ca	45.5	38.4	1.0	0.6	1.1			40.5	4.7
Fe^{2+}	1.0					1.0		1.0	
Fe^{3+}									
V^{4+}	1.1		0.6					0.6	
V^{5+}				0.5				0.5	
Si	13.7	13.5				0.3		13.7	
P^{5+}	0.59				0.59			0.59	
O	35.7	30.6	0.8	0.6	1.2	0.6		35.0	1.8
	Meas. A.4	**Ca_2SiO_4**	**Ca_2VO_4**	**$Ca_3(VO_4)_2$**	**$Ca_3(PO_4)_2$**	**Fe_2SiO_4**	**Ca_2CrO_4**	**Opt.**	**CaO**
F		0.282071	0.577020	0.038969	0.035905	0.014595	0.018957		0.021793
Ca	41.9	13.1	23.7	1.3	1.4		0.8	40.3	1.6
Fe^{2+}	0.8					0.8		0.8	
Fe^{3+}									
V^{4+}	16.2		15.1					15.1	
V^{5+}				1.1				1.1	
Si	4.8	4.6				0.2		4.8	
P^{5+}	0.72				0.72			0.72	
Cr^{4+}	0.50						0.50	0.50	
O	32.8	10.5	18.9	1.4	1.5	0.5	0.6	33.4	0.6

3.3.2. Modeling of the Composition of the Different Grain Types—Characterization of DFS

The type D grains (Figure 1) are best characterized by a dicalcium ferrite-like structure. The composition of the individual D-type grains is mostly constant. The average elemental concentrations and the spread expressed as the standard deviation of these grains are given in Table 6.

Based on the Ca/Fe ratio (D.1-D.3 Table 6), $Ca_2Fe_2O_5$ can be identified as the main structure. Pure dicalcium ferrite contains 29.487 wt.% Ca, 41.087 wt.% Fe, and 29.426 wt.% O. Except for iron with a lower-than-expected concentration by 18 wt.% (Table 6), the measurement results are relatively close (deviation around 1 wt.%) to the ideal composition for calcium and oxygen in dicalcium ferrites. Additionally, standard deviations for the iron content (calculated from at least 7 individual values) are also relatively high, between 0.05 to 3 wt.%.

Table 6. Average concentrations of main elements (in wt.%) in different DFS-grains (D.1-D.3), measured with EPMA, WDX (standard deviation in brackets (N = 7)). As a comparison, composition of pure dicalcium ferrite is listed as well.

Grain	D.1	D.2	D.3	Ideal $Ca_2Fe_2O_5$
Ca	30.5 (0.3)	31.3 (0.8)	30.50 (0.03)	29.49
Fe	28 (2)	24 (3)	27.08 (0.05)	41.09
Ti	3.0 (0.8)	4.0 (1.1)	3.0 (0.3)	-
V	2. 8 (0.2)	3.0 (0.205)	2.92 (0.06)	-
Cr	1.1 (0.8)	2.2 (1.0)	1.1 (0.2)	-
Al	2.4 (0.2)	2.3 (0.4)	2.37 (0.04)	-
Mn	0.55 (0.04)	0.56 (0.06)	0.52 (0.02)	-
O	27.0 (0.7)	27.4 (0.4)	26.86 (0.11)	29.43

According to the elemental determination, the DFS incorporates titanium, vanadium, chromium, and aluminum in addition to the major elements calcium, iron, and oxygen into its structure. Especially, aluminum and vanadium exhibit relatively constant concentrations in all measurements. Higher variations occur in the content of titanium and chromium. Following similar procedures described in Section 2.2.4, a structural formula based on the O_5-structure of dicalcium ferrite is calculated. For the calculation of the DFS stoichiometry, a solid solution of the following virtual components: $Ca_2Fe_2O_5$, Ca_2FeAlO_5, Ca_2FeTiO_5, Ca_2AlVO_5, Ca_2CrFeO_5, and Ca_2AlMnO_5 is assumed. Again, the selection is based on the structural similarity to the crystal system of DFS. The respective fractions were calculated for each of the virtual components, and the result was then normalized to five oxygen atoms (based on the O_5-structure of $Ca_2Fe_2O_5$). Details on the measurement results and the calculated fraction of all virtual components for D.1 can be found in Table 7, leading to a uniform stoichiometric formula:

$$Ca_2\ (Fe^{3+}{}_{1.39},\ Al^{3+}{}_{0.22},\ V^{3+}{}_{0.13},\ Ti^{3+}{}_{0.17},\ Cr^{3+}{}_{0.06},\ Mn^{3+}{}_{0.02})_2\ O_5$$

Table 7. Calculated fractions of virtual components postulated from elemental composition determined by EPMA analysis of grains of D.1-type (DFS-grain). First column: measured concentrations; F: fraction of virtual compound. Excess Ca is calculated as CaO.

	Meas. D.1	Ca_2Fe2O_5	Ca_2FeAlO_5	Ca_2FeTiO_5	Ca_2AlVO_5	Ca_2CrFeO_5	Ca_2AlMnO_5	Opt.	CaO
F		0.534560	0.059061	0.165283	0.130859	0.056696	0.024145		0.012059
Ca	30.5	15.8	1.9	5.0	4.4	1.7	0.8	29.6	0.9
Fe^{3+}	28.0	22.0	1.34	3.5		1.2		28.0	
V^{3+}	2.8				2.8			2.8	
Al^{3+}	2.4		0.7		1.4		0.3	2.4	
Cr^{3+}	1.1					1.1		1.1	
Ti^{3+}	3.0			23.0				3.0	
Mn^{3+}	0.55						0.55	0.55	
O	27.00	15.7	1.9	5.0	4.4	1.7	0.8	29.6	0.3

The complete calculations for the other grains (D.2, D.3) are listed in the Appendix A. Here, only 0.9 wt.% of Ca were unaccounted for.

4. Discussion

For many different reasons, vanadium-containing BOF slags are coming into focus in research, industry, and legislation. The most important points are the possible recovery of vanadium for reuse in, e.g., battery technology, but also the toxicity of its various compounds. Both recovery and toxicity management requires a basic understanding of vanadium chemistry in BOF slags, especially regarding its distribution among certain host phases and the occurring oxidation states. Based on measurements and modeling, this study provides an approach addressing these important questions.

4.1. Vanadium Host Compounds—COS and DFS

EPMA data show that vanadium occurs mainly in COS (divided in COS-Si type and COS-V type) and less in DFS, which is in good agreement with previous studies, e.g., [14,15]. In those studies, vanadium was mainly present in the two slag compounds, calcium orthosilicate and dicalcium ferrite, with a vanadium mass content of 0.52–1.03 wt.% or 0.44–1.14 wt.%, respectively. The vanadium content in similar phases found in this study is slightly higher for DFS (2–3 wt.% in maximum). In the case of COS, the observed vanadium incorporation was partly significantly higher regarding the COS-V type, up to 18 wt.%).

Looking at the vanadium distribution in COS, firstly, it is noticeable that two extremes occur here, which to the best of our knowledge were not described previously. On the one hand, nearly pure Ca_2SiO_4, was determined. This phase contains only about 1 wt.% vanadium (COS-Si type, Table 4, A.1, A.2). On the other hand, vanadium can substantially be enriched with a maximum analyzed vanadium concentration of 18 wt.% (COS-V type, Table 4, A.3, A.4). In the investigated slag, only these two variations of COS are determined. In-between phases exhibiting a continuous concentration gradient were not observed. In addition to vanadium, small amounts of phosphorus are also incorporated into both COS types. The connection between vanadium and phosphorous in calcium orthosilicates was already observed by other authors, e.g., [14,20,22]. Preßlinger and Klepp [14], for example, described a coexistence of P^{5+} and V^{5+} in calcium orthosilicate phases, in addition to Al^{3+} and Ti^{4+}. While Wu et al. [22] for slags with comparable basicity to the slags in this study (basicity = 3 in [22], basicity = 3.8 in this study), observe incorporation of vanadium and phosphorous into calcium orthosilicates in a ratio of approx. one to one (P_2O_5 = 5.42 wt.% and V_2O_5 = 5.65 wt.% [22]). In DFS, neither a gradient in the vanadium distribution nor two endmembers occur. Throughout all measurements, DFS shows a constant content of vanadium, with some fluctuations in chromium and titanium. A possible reason for this observation could be a limitation of the vanadium incorporation into DFS to *approx.* 3 wt.%. Therefore, an incomplete solid solution could be assumed.

4.2. Modeling

The modeling in this study should estimate the lattice positions vanadium will occupy and in which oxidations states it will occur in slags. Based on these hypotheses, a potential stoichiometric formula is proposed. Knowledge about possible oxidation states and positions in the respective hosts serves as a starting point for future experiments.

The PXRD and EPMA results strongly support a majority of grains having the general stoichiometric formula and crystal lattice of Ca_2SiO_4. It can be used as a starting point to calculate the COS composition with the generalized formula X_2YO_4 with X = Ca, less Fe^{2+} and Y = Si,V($^{4+}$/$^{5+}$), less P or Cr^{4+} using virtual components (Table 5).

Excess Ca from the measurement compared to the calculated virtual solid solution $(Ca_{1.91}, {Fe^{2+}}_{0.04})_{1.95}$ $({V^{4+}}_{0.02}, {V^{5+}}_{0.04}, {P^{5+}}_{0.06}, Si_{0.88})_{1.0}$ O_4 is listed as CaO (free lime) in Table 5. This excess Ca content is significantly higher in the COS-Si type compared to the COS-V type. Wachsmut et al. [23] describe the different forms of free lime (CaO) in BOF slags. Besides residual free lime, in the form of spongy aggregates, it also occurs as a very fine particulate in an intimate mixture with calcium orthosilicates. Tricalcium silicate, which can occur in slags as a high-temperature phase, unstable at room temperature,

decomposes around 1250 °C [24] to calcium orthosilicate and free lime (CaO). Therefore, the above-mentioned intimate mixture of CaO and calcium orthosilicates is likely to result from the solid-state decomposition of tricalcium silicate.

The occurrence of submicrocrystalline domains of pure CaO (free-lime), which are not resolvable with EPMA is plausible, and therefore the COS-Si type and the COS-V type can be expressed as:

$$\text{COS-Si: } (Ca_{1.91}, Fe^{2+}{}_{0.04})_{1.95}\ (V^{4+}{}_{0.02}, V^{5+}{}_{0.04}, P^{5+}{}_{0.06}, Si_{0.88})_{1.0}\ O_4 + nCaO$$

$$\text{COS-V: } (Ca_{1.90}, Fe^{2+}{}_{0.03})_{1.93}\ (V^{4+}{}_{0.55}, V^{5+}{}_{0.07}, P^{5+}{}_{0.07}, Cr^{4+}{}_{0.02}, Si_{0.28})_{1.0}\ O_4 + nCaO$$

The higher CaO content calculated for COS-Si compared to that of COS-V can be explained by the hypothesis COS-Si being a primarily solidifying phase, leading to a higher amount of the high-temperature phase tricalcium silicate originally present.

The calculations indicate that in the COS-V type, vanadium occupies the silicon position as both V^{5+} and V^{4+} with a calculated ratio of 7:93 (V^{5+}:V^4). In the COS-Si type vanadium also seems to occupy the silicon position as V^{5+} and V^{4+}, with a calculated ratio of 45:55 (V^{5+}:V^4). According to the same modeling principle, the other incorporated impurities can be estimated as well: together with chromium, phosphorous also occupies the silicon position. Additionally, the calculations indicate that small amounts of Fe^{2+} can occupy the calcium position. The incorporation of pentavalent vanadium and phosphorus on the silicon position leads to a charge excess which seems to be compensated by point defects on the calcium position. Rapid cooling of the slags prevents ideal segregation of the individual atoms; a certain disorder remains, which is then compensated by imperfections. Comparing the low vanadium concentrations in A.1 and A.2 with the high vanadium concentrations in A.3 and A.4, A.1, and A.2 represent nearly pure Ca_2SiO_4 (predicted formula: $(Ca_{1.91}, Fe^{2+}{}_{0.04})_{1.95}(V^{4+}{}_{0.02}, V^{5+}{}_{0.04}, P^{5+}{}_{0.06}, Si_{0.88})_{1.0}O_4$ compared to that of Ca_2SiO_4). In contrast, the V-enriched grains A.3 and A.4 with the predicted stoichiometry $(Ca_{1.90}, Fe^{2+}{}_{0.03})_{1.93}$ $(V^{4+}{}_{0.55}, V^{5+}{}_{0.07}, P^{5+}{}_{0.07}, Cr^{4+}{}_{0.02}, Si_{0.28})_{1.0}O_4$ show a significant deviation.

Regarding DFS, the stoichiometric formula $Ca_2Fe_2O_5$ can be used to start modeling with virtual components. The calculations estimate vanadium occupying the Fe^{3+}-position as V^{3+}, together with Al^{3+}, $Cr^{3+,}$ and Ti^{3+}. Similar to COS, a relatively small amount of excess Ca is calculated in the virtual solid solution (Table 7). Again, referring to Wachsmut et al. [23], free lime can occur in BOF-slags as precipitates along the grain boundaries of dicalcium ferrites, assuming the excess Ca content arises from crystalline CaO deposited at the grain boundaries and co-measured. The calculated DFS can be expressed as follows:

$$Ca_2(Fe^{3+}{}_{1.39}, Al^{3+}{}_{0.22}, V^{3+}{}_{0.13}, Ti^{3+}{}_{0.17}, Cr^{3+}{}_{0.06}, Mn^{3+}{}_{0.02})_2O_5 + nCaO$$

4.3. Critical Evaluation of the Virtual Component Modeling Results

The main influencing factors defining impurity incorporations into a crystal lattice must be considered regarding the plausibility of the virtual component modeling. The radii deviations of different ions in connection with theories of mineral-melt partitioning describe to what extent a replacement is possible. The crystallization path during solidification describes the chronological order when impurities can be incorporated, and the redox behavior explains which species can occur in the melt.

Based on the modeling in this study, vanadium seems to replace silicon in COS on the one hand and iron in DFS on the other hand. This replacement must be possible regarding ionic radii and mineral-melt partitioning behavior in the first place.

Understanding vanadium affinities in natural processes may be helpful as a basis for the behavior of vanadium in industrially produced melts, such as BOF slag.

The theory on mineral-melt partitioning underlying segregation effects can be applied to predict elemental solidification from slag melts. It strongly depends on the size of the respective ion. The ionic radii and their ratios of the elements define if incorporation is in accordance with lattice spacings or interatomic distances. If two ions of the same

charge with a slight difference in the ionic radius are considered, both will be incorporated with a chronological difference. For the larger ion, the bonds are weakened, lowering the melting point. In this case, the slightly smaller ion is incorporated first, resulting in an accumulation of the slightly larger ion in the mother liquor. If two ions of the same size compete for a certain lattice site, the ion with the higher charge is preferentially incorporated [25]. The ionic radii of e.g., V^{5+} and Si^{4+} are quite different: Si^{4+} (IV) = 0.026 nm, V^{5+} (IV) = 0.0355 nm while the coordination (shown in brackets) is the same. Since the ionic radii in solids depend strongly on the respective coordination, it also needs considering. However, incorporation may still be possible due to the loosening of interatomic bonds. Regarding DFS, an exchange of Fe^{3+} (VI) = 0.0645 nm by V^{3+} (VI) = 0.064 nm is likely to occur [26].

4.3.1. Presence of V^{3+}, V^{4+}, and V^{5+}

Regarding the oxidation states of vanadium in slags, in this study, a coexistence of V^{3+}, $V^{4+,}$ and V^{5+} is postulated, where V^{3+} occupies the Fe^{3+} position of DFS and V^{4+} and V^{5+} occupy the Si^{4+} position in COS. According to literature, vanadium in slags is mainly present as the two redox pairs V^{3+}/V^{4+} or V^{4+}/V^{5+}, depending on the slag composition and the oxygen partial pressure. A main influencing factor correlated to the slag composition is the basicity of the slag since basic components produce free O^{2-} ions, resulting in higher oxygen availability. At high temperatures, the coexistence of all three species is possible, whereby some authors postulate only two species can be present in the liquid slag, either V^{3+}/V^{4+} or V^{4+}/V^{5+} [10,27,28].

According to *Farah* [29], there is a region of coexistence of the two redox pairs in the melt, at oxygen potentials between 10^{-4}–10^{-6} atm., whereas this region of coexistence increases with increasing basicity (the basicity with the coexistence of all three vanadium species being CaO/SiO_2 = 1.23 according to [29]). Furthermore, a decrease in the V^{3+}/V^{4+} and V^{4+}/V^{5+} ratio with increasing oxygen partial pressure as well as with increasing basicity is observed [30]. Both assumptions suggest that at the beginning of the solidification, when the basicity of the slag is equal to the initial basicity (CaO/SiO_2 = 3.8 in this study) and oxygen partial pressure is highest, immediately after the blowing process, V^{4+}/V^{5+} is lowest and V^{3+} concentrations negligible. This theory is supported by considering the crystallization path: the COS solidifying at the beginning incorporates a higher amount of V^{5+} into the lattice (COS-Si type, approx. 1 wt.%), leading to decreasing basicity. Due to progressive crystallization and with decreasing pO_2 and temperature, the V^{4+}/V^{5+} ratio increases, and vanadium enriches in the melt. This leads to the incorporation of V^{4+} and V^{5+} into the COS at a later stage, with a balance clearly on the V^{4+} side, whereby the incorporation of V^{5+} is still preferred over V^{4+} due to the higher charge. At this point, towards the end of the crystallization of COS when crystallization along the three-phase coexistence line with DFS takes place, the vanadium accumulation in the residual melt leads to a concentration exceeding the remaining Si^{4+} concentration. As a result, proportionally large amounts of vanadium, $V^{4+,}$ and a minor fraction of V^{5+} are incorporated into the COS lattice (COS-V type, up to 18 wt.%). In this stadium, V^{3+} becomes thermodynamically stable. Subsequently, it is assumed DFS incorporates the maximum amount of vanadium (approx. 3wt.% entirely as V^{3+}) as allowed by the lattice constraints.

4.3.2. Ferrous Iron Next to Pentavalent Vanadium

In the calculated universal stoichiometric formulas of the COS-V and COS-Si types $(Ca_{1.90}, Fe^{2+}{}_{0.03})_{1.93}$ $(V^{4+}{}_{0.55}, V^{5+}{}_{0.07}, P^{5+}{}_{0.07}, Cr^{4+}{}_{0.02}, Si_{0.28})_{1.0}O_4$, $(Ca_{1.91}, Fe^{2+}{}_{0.04})_{1.95}$ $(V^{4+}{}_{0.02}, V^{5+}{}_{0.04}, P^{5+}{}_{0.06}, Si_{0.88})_{1.0}$ O_4) it is noticeable that part of the calcium lattice position is assumed to be occupied by ferrous iron, Fe^{2+}. However, the vanadium species indicate a relatively strong oxidation environment. In this environment, the abundance of ferric iron would be more plausible. *Park* et al. [31] postulated, at the beginning of the solidification directly after tapping, the Fe^{2+}/Fe^{3+} is determined by the initial Fe content of the slag as well as by its basicity. Considering these results with respect to high basicities (as they occur in the BOF

slag of this study), at the beginning of the crystallization, when basicity is highest, only a very small proportion of Fe^{2+} but still plausible is present in the melt with the equilibrium clearly on the Fe^{3+} side. This observation is consistent with the assumptions in this study to the extent that a small amount of Fe^{2+} (*approx.* 1 wt.%) is first incorporated into the COS lattice, followed by crystallization of DFS, incorporating Fe^{3+} (*approx.* 27 wt.%). Since iron appears in all measurements of the COS grains and the calcium position in the orthosilicates is known to be occupied by Fe^{2+} (e.g., in Fe_2SiO_4), an occurrence as Fe^{2+} is most likely. Another explanation for the measured Fe content would be the presence of submicrocrystalline, finely distributed Fe^{3+}-oxide needles, which cannot be resolved in the EPMA analytics used.

5. Conclusions

In this study, high vanadium-containing BOF slags were investigated to define potential host phases for vanadium. With EPMA it is observed that vanadium accumulates preferentially in COS (calcium orthosilicate-like compound) but is also incorporated in DFS (dicalcium ferrite solid solution). The primitive oxides contain no vanadium. The possible valence state is of great importance regarding the leaching behavior of the element. Therefore, the compositions were estimated by modeling with virtual components. These calculations show that the incorporation of vanadium into COS seems to take place in two different ways: in an early stage of the solidification, one endmember incorporates relatively small amounts of vanadium (~1 wt.%, divided into 93% V^{4+} and 7% V^{5+}) into its crystal lattice on the silicon position (COS-Si type). In a later stage and with increasing relative enrichment of vanadium in the melt and decreasing basicity, a high vanadium calcium orthosilicate (COS-V type) with an exemplary V^{4+}/V^{5+} ratio of 55/45, both occupying the silicon position, is crystallizing. In contrast to the general principle of coupled substitution, in this study, substitution of Si^{4+} by V^{3+} in connection with $V^{5+}(/P^{5+})$ is not plausible. It is assumed that the incorporation of V^{4+} and V^{5+} is leading to a charge excess on the silicon position, which is compensated by an under-occupied calcium position. The vanadium incorporation into DFS follows the same pattern throughout the whole sample. Here, trivalent vanadium seems to be incorporated on the iron position at a level of 3 wt.%.

The hypothetic stoichiometry and oxidation states determined in this study need further experimental proof in the future. The relatively low content of vanadium (compared to other, e.g., V^{5+} carriers) and the diversity of the sample (matrix) complicate the analysis via XANES on a laboratory scale. Therefore, the EPMA results but especially the modeling assumptions in this study, serve as a basis for future μ-XANES and μ-XRD investigations. In addition, based on the results postulated here regarding the oxidation state, the leaching behavior of vanadium can be studied and compared.

Author Contributions: S.W., T.S., U.E.A.F. conceived the paper; S.W. conducted the literature review; all experiments were designed and performed by S.W.; the phase analysis (PXRD and EPMA) and the mineralogical investigation were conducted by S.W. and T.S.; interpretation and discussion were conducted by all authors. All authors have read and agreed to the published version of the manuscript.

Funding: This research received no external funding.

Acknowledgments: We acknowledge support by Open Access Publishing Fund of Clausthal University of Technology.

Conflicts of Interest: The authors declare no conflict of interest. The funders had no role in the design of the study; in the collection, analyses, or interpretation of data; in the writing of the manuscript, or in the decision to publish the results.

Appendix A

	Meas. A.1	Ca_2SiO_4	Ca_2VO_4	$Ca_3(VO_4)_2$	$Ca_3(PO_4)_2$	Fe_2SiO_4		Opt.	CaO
F		0.813379	0.027384	0.020103	0.028910	0.017558			0.063008
Ca	45.3	37.9	1.1	0.7	1.1			40.8	4.5
Fe^{2+}	0.96					0.96		0.96	
Fe^{3+}									
V^{4+}	1.3		0.7					0.7	
V^{5+}				0.6				0.6	
Si	13.5	13.3				0.2		13.5	
P^{5+}	0.58				0.58			0.58	
O	35.4	30.2	0.9	0.7	1.2	0.6		33.7	1.8
	Meas. A.3	**Ca_2SiO_4**	**Ca_2VO_4**	**$Ca_3(VO_4)_2$**	**$Ca_3(PO_4)_2$**	**Fe_2SiO_4**	**Ca2CrO4**	**Opt.**	**CaO**
F		0.296813	0.591268	0.039931	0.035279	0.010947	0.019858		0.000573
Ca	41.7	13.8	24.3	1.4	1.4		0.8	41.7	0.04
Fe^{2+}	0.6					0.6		0.6	
Fe^{3+}									
V^{4+}	16.6		15.4					15.4	
V^{5+}				1.2				1.2	
Si	4.89	4.8				0.2		4.99	
P^{5+}	0.70				0.70			0.70	
Cr^{4+}	0.526						0.526	0.526	
O	32.8	11.0	19.4	1.5	1.5	0.4	0.7	34.4	0.02
	Meas. D.2	**Ca_2Fe2O_5**	**Ca_2FeAlO_5**	**Ca_2FeTiO_5**	**Ca_2AlVO_5**	**Ca_2CrFeO_5**	**Ca_2AlMnO_5**	**Opt.**	**CaO**
F		0.390686	0.040088	0.220377	0.140206	0.113393	0.024584		0.058106
Ca	31.3	11.5	1.3	6.7	4.7	3.4	0.8	28.5	4.2
Fe^{2+}	24.0	16.1	0.9	4.7		2.4		24.0	
V^{3+}	3.0				3.0			3.0	
Al^{3+}	2.3		0.4		1.6		0.3	2.3	
Cr^{3+}	2.2					2.2		2.2	
Ti^{3+}	4.0			4.0				4.0	
Mn^{3+}	0.56						0.56	0.56	
O	27.4	11.5	1.3	6.7	4.7	3.4	0.8	28.4	1.7
	Meas. D.3	**Ca_2Fe2O_5**	**Ca_2FeAlO_5**	**Ca_2FeTiO_5**	**Ca_2AlVO_5**	**Ca_2CrFeO_5**	**Ca_2AlMnO_5**	**Opt.**	**CaO**
F		0.516164	0.051918	0.165283	0.136467	0.056696	0.022828		0.020915
Ca	30.5	15.2	1.7	5.0	4.6	1.67	0.8	29.00	1.50
Fe^{2+}	27.08	21.2	1.2	3.50		1.18		27.08	
V^{3+}	2.92				2.92			2.92	
Al^{3+}	2.37		0.57		1.55		0.25	2.37	
Cr^{3+}	1.1					1.1		1.1	
Ti^{3+}	3.0			3.0				3.0	
Mn^{3+}	0.52						0.52	0.52	
O	26.86	15.2	1.71	5.01	4.59	1.69	0.76	28.94	0.60

References

1. Worldsteel Association. *2020 World Steel in Figures*; Worldsteel Association: Brussels, Belgium, 2020; pp. 11–12.
2. Preßlinger, H.; Mayr, M.; Apfolterer, R. Quantitative phase evaluation of converter slags. *Steel Res.* **1999**, *70*, 209–214. [CrossRef]
3. Aarabi-Karasgani, M.; Rashchi, F.; Mostoufi, N.; Vahidi, E. Leaching of vanadium from LD converter slag using sulfuric acid. *Hydrometallurgy* **2010**, *102*, 14–21. [CrossRef]
4. Kelley, K.D.; Scott, C.T.; Polyak, D.E.; Kimball, B.E. *Vanadium*; Schulz, K.J., DeYoung, J.H., Jr., Seal, R.R., II, Bradley, D.C., Eds.; U.S. Geological Survey Professional Paper 1802; Critical Mineral Resources of the United States-Economic and Environmental Geology and Prospects for Future Supply: Reston, VA, USA, 2017; pp. U1–U36.
5. Pourret, O.; Dia, A. *Encyclopedia of Geochemistry*; White, B., Casey, W., Goldstein, S., Harnett, H., Marty, B., Yurimoto, H., Eds.; Chapter Vanadium; Springer: Deutschland, Germany, 2018; pp. 1474–1476. [CrossRef]
6. Holleman, A.F.; Wiberg, N.; Wiberg, E. Lehrbuch der Anorganischen Chemie. Walter de Gruyter: Berlin, Germany, 2007. [CrossRef]
7. Toplis, M.J.; Corgne, A. An experimental study of element partitioning between magnetite, clinopyroxene and iron-bearing silicate liquids with particular emphasis on vanadium. *Contrib. Miner. Petrol.* **2002**, *144*, 22–37. [CrossRef]
8. Righter, K.; Leeman, W.P.; Hervig, R.L. Partitioning of Ni, Co and V between spinel-structured oxides and silicate melts: Importance of spinel composition. *Chem. Geol.* **2006**, *227*, 1–25. [CrossRef]

9. Schreiber, H. An electrochemical series of redox couples in silicate melts: A review and applications to geochemistry. *J. Geophys. Res.* **1987**, *92*, 9225. [CrossRef]
10. Inoue, R.; Suito, H. Distribution of Vanadium between Liquid Iron and MgO-saturated Slags of the System CaO-MgO-FeO_x&SiO_2. *Tetsu-to-Hagane* **1982**, *68*, 1532–1540. [CrossRef]
11. Zeng, Q.; Li, J.; Yu, Y.; Zhu, H. Effect of Cooling Rate on Crystallization Behavior of CaO-SiO2-MgO-Cr2O3 Based Slag. *High Temp. Mater. Process.* **2020**, *39*, 74–80. [CrossRef]
12. Hobson, A.J.; Stewart, D.I.; Bray, A.W.; Mortimer, R.J.G.; Mayes, W.M.; Rogerson, M. Mechanism of Vanadium Leaching during Surface Weathering of Basic Oxygen Furnace Steel Slag Blocks: A Microfocus X-ray Absorption Spectroscopy and Electron Microscopy Study. *Environ. Sci. Technol.* **2017**, *51*, 7823–7830. [CrossRef]
13. Wu, F.; Qin, T.; Li, X.; Liu, Y.; Huang, J.-H.; Wu, Z. First-principles investigation of vanadium isotope fractionation in solution and during adsorption. *Earth Planet. Sci. Lett.* **2015**, *426*, 216–224. [CrossRef]
14. Preßlinger, H.; Klepp, K.O. Vanadium in converter slags. *Steel Res.* **2016**, *73*, 522–525. [CrossRef]
15. Hobson, A.J.; Stewart, D.I.; Bray, A.W.; Mortimer, R.J.G.; Mayes, W.M.; Riley, A.L. Behaviour and fate of vanadium during the aerobic neutralisation of hyperalkaline slag leachate. *Sci. Total Environ.* **2018**, *643*, 1191–1199. [CrossRef] [PubMed]
16. Dill, H.G. The "chessboard" classification scheme of mineral deposits: Mineralogy and geology from aluminum to zirconium. *Earth-Sci. Rev.* **2010**, *100*, 1–420. [CrossRef]
17. Rodriguez-Carvajal, J. Recent advances in magnetic structure determination by neutron powder diffraction. *Phys. B: Condens. Matter* **1993**, *192*, 55–69. [CrossRef]
18. Merlet, C. Quantitative Electron Probe Microanalysis: New Accurate Φ (ρz) Description. In *Electron Microbeam Analysis*; Springer: Vienna, Austria, 1992; pp. 107–115. [CrossRef]
19. Grazulis, S.; Chateigner, D.; Downs, R.T.; Yokochi, A.F.T.; Quirós, M.; Lutterotti, L.; Manakova, E.; Butkus, J.; Moeck, P.; Le Bail, A. Crystallography Open Database—An open-access collection of crystal structures. *J. Appl. Crystallogr.* **2009**, *42*, 726–729. [CrossRef]
20. Saalfeld, H. Kristallchemische Untersuchungen im System Ca_2SiO_4–$Ca_3(PO_4)_2$. Beitrag zur Frage der Diadochie des Siliciums und Phosphors. *Z. Krist.-Cryst. Mater.* **1971**, *197*, 133. [CrossRef]
21. McConnell, D.; Verhoek, F. Crystals, minerals and chemistry. *J. Chem. Educ.* **1963**, *40*, 512. [CrossRef]
22. Wu, X.; Li, L.; Dong, Y. Enrichment and crystallization of vanadium in factory steel slag. *Metallurgist* **2011**, *55*, 401–409. [CrossRef]
23. Wachsmuth, F.; Geiseler, J.; Fix, W.; Koch, K.; Schwerdtfeger, K. Contribution to the Structure of BOF-Slags and its Influence on Their Volume Stability. *Can. Metall. Q.* **1981**, *20*, 279–284. [CrossRef]
24. Mohan, K.; Glasser, F.P. The thermal decomposition of Ca_3SiO_5 at temperatures below 1250 °C I. Pure C_3S and the influence of excess CaO or Ca_2SiO_4. *Cem. Concr. Res.* **1977**, *7*, 1–7. [CrossRef]
25. Goldschmidt, V.M. The principles of distribution of chemical elements in minerals and rocks. The seventh Hugo Müller Lecture, delivered before the Chemical Society on March 17th. *J. Chem. Soc.* **1937**, 655–673. [CrossRef]
26. Shannon, R.D. Revised effective ionic radii and systematic studies of interatomic distances in halides and chalcogenides. *Acta Crystallogr. Sect. A* **1976**, *32*, 751–767. [CrossRef]
27. Mittelstadt, R.; Schwerdtfeger, K. The dependence of the oxidation state of vanadium on the oxygen pressure in melts of VOx, Na2O-VOx, and CaO-SiO2-VOx. *Metall. Trans. B* **1990**, *21*, 111–120. [CrossRef]
28. Sakkas, K.; Kapelar, S.; Panias, D.; Nomikos, P.; Sofianos, A. *Slag Atlas*, 2nd ed.; Verlag Stahleisen GmbH: Düsseldorf, Germany; Deutschland, Germany, 1995; pp. 10–19.
29. Farah, H. Oxidation-reduction equilibria of vanadium in CaO-SiO_2, CaO-Al_2O_3-SiO_2 and CaO-MgO-SiO_2 melts. *J. Mater. Sci.* **2003**, *38*, 1885–1894. [CrossRef]
30. Wang, H.; Wang, L.; Seetharaman, S. Determination of Vanadium Oxidation States in CaO-MgO-Al_2O_3-SiO_2-VOx System by K Edge XANES Method. *Steel Res. Int.* **2016**, *87*, 199–209. [CrossRef]
31. Park, J.M. Iron redox equilibria in BOF slag equilibrated with ambient air. *Steel Res.* **2002**, *73*, 39–43. [CrossRef]